Particle Motion from Offshore Impact Piling Including Pile–Soil Linear Contact Slip

Khairina A. Canny, Yaxi Peng, Athanasios Tsetas, and Apostolos Tsouvalas

Contents

Abstract

Besides the underwater sound generated by offshore pile-driving, particle motion near the seabed can be detected by many marine species, raising concerns about ecological effects. Both particle motion and underwater noise may influence the behavior and health of organisms sensitive to these disturbances. These potential impacts highlight the importance of predictive models that represent the interactions between the pile, the soil, and the seawater. This case study examines how pile–soil contact during impact pile-driving may affect particle motions in the seawater column and the seabed. In reality, the pile–soil interaction in the process of pile-driving is nonlinear. However, a linear equivalent representation allows one to investigate, to a reasonable extent, the effects on the acoustoelastic waves generated in the soil–water domain. Linear springs and dashpots are therefore introduced at the pile–soil interface, allowing relative motions to develop

OPEN ACCESS with major support from JASCO APPLIED SCIENCES

K. A. Canny (✉) · Y. Peng · A. Tsetas · A. Tsouvalas
Civil Engineering and Geoscience, Delft University of Technology, Delft, The Netherlands
e-mail: k.a.c.canny@tudelft.nl; y.peng@tudelft.nl; a.tsetas@tudelft.nl; a.tsouvalas@tudelft.nl

A. N. Popper et al. (eds.), *The Effects of Noise on Aquatic Life IV*,
https://doi.org/10.1007/978-3-031-94229-7_32-1

between the soil and the pile, that is, linear contact slip is introduced. A case study is conducted to evaluate the implications of pile slip on vibroacoustic behavior, with a particular focus on the resulting particle motion trajectories in the vicinity of the seabed. The findings of this study are presented alongside the potential perceptibility and sensitivity of vibrations by marine species.

Keywords

Pile driving · Fluid–soil–structure interaction · Linear contact slip · Particle motion

Introduction

The rapid expansion of offshore renewable energy has driven significant growth in the size of wind turbine monopile foundations. The increase in monopile diameter leads to dynamic excitations at lower frequencies, where accurate prediction of the resulting acoustic field and soil vibration requires detailed characterization of the soil behavior and the pile–soil dynamic interaction.

Marine sediments show great variability while, in some cases, the upper soil is composed of soft unconsolidated sediments that are typically characterized by large uncertainty when it comes to dynamic soil properties. Importantly, similar uncertainties may arise in stiff upper soil layers if their dynamic properties (e.g., small-strain stiffness, damping, shear-wave velocity) are not properly identified. These geotechnical uncertainties complicate the prediction of the energy transfer into the soil and in the seawater during impact pile-driving. Of particular concern is low-frequency particle motion in benthic zones, which is detectable by marine organisms and can influence their behavior and cause physiological stress or lead to injury (Solé et al. 2017, 2023). While particle motion is increasingly recognized as an important ecological factor, most predictive models focus on sound pressure levels and assume idealized, perfect contact pile–soil interfaces (Peng et al. 2021; Tsouvalas and Metrikine 2014). It is important to note that while the aforementioned models, which assume no soil–pile slip, may be able to predict the sound levels in the seawater with high accuracy, the same may not hold true when it comes to the prediction of the particle velocity trajectories (both in the seabed and in the seawater) because the latter are highly sensitive to the exact vibration pattern of the pile and the soil–water in its vicinity.

Tsetas et al. (2023) introduced a history-dependent frictional contact model between the pile and soil in a semi-analytical framework for vibratory pile-driving that captures the nonlinear soil–pile interaction. Molenkamp et al. (2024) expanded this by coupling the pile–soil interaction with the surrounding fluid using a boundary element method. Bohne et al. (2024) incorporated contact mechanisms in FEM simulations for small impact-driven piles. All these studies have demonstrated that the vibration amplitudes close to the seabed surface and in the soil are highly sensitive to the pile–soil interface formulation. However, there remains a research gap in modeling particle motion effects resulting from realistic pile–soil contact in large-diameter monopiles.

To address this gap, a predictive model is developed to explicitly account for axial pile–soil interaction. Using a Kelvin–Voigt framework, the pile–soil interface is represented as a linear spring–dashpot system, capturing both stiffness and damping. This interface allows relative vertical displacement at the interface, improving interaction mechanical properties and enabling more accurate estimation of particle motion near the seabed. This study examines how pile–soil contact during impact pile-driving affects particle motion in the vicinity of the seabed. Although the interface between pile and soil is inherently nonlinear, a linear equivalent representation enables study of its influence on the acoustoelastic waves generated in both soil and fluid domains.

The outline of this chapter is as follows. In section "Model Description and Governing Equations," the proposed model is described, and the governing equations for the axisymmetric case are formulated. Secondly, a case study is presented that examines the effects of soil linear contact slip between pile and soil on particle motion, supported by sensitivity analyses across different contact scenarios. Finally, the main findings are presented, their potential ecological significance discussed, and the conclusion and future research directions outlined.

Model Description and Governing Equations

The entire set of subsystems of the pile-driving mechanism is depicted in Fig. 1 that consists of the pile, modeled as a thin-shell structure, the seawater modeled as a linear acoustic fluid, and the soil domain modeled as a linear elastic continuum, that is, the vibroacoustic system under consideration. These subsystems are defined in cylindrical coordinates and assumed to be axisymmetric in both geometry and the force loading (f_e) applied at the pile head. The fluid is considered as a three-

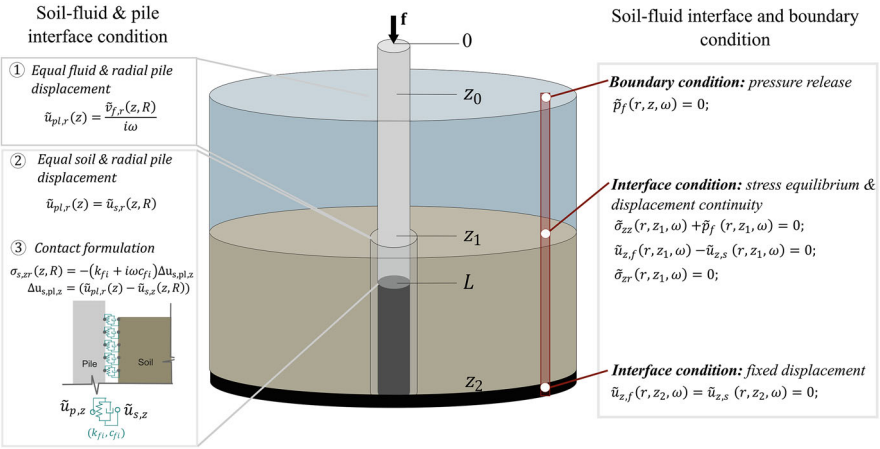

Fig. 1 The model description for fluid-soil–pile interaction, soil–fluid interface and boundary conditions, and soil–fluid–pile interface condition, including the contact interface representation using elastic spring–dashpot system

dimensional, inviscid, and compressible medium of compressional wave speed c_f and fluid density ρ_f. The fluid domain ranges from $z_0 < z < z_1$, where z_0 denotes the sea surface and z_1 the seabed level. The soil is characterized by its density (ρ_s), the compressional wave velocity (c_p), and the shear wave velocity (c_s). The soil domain extends from the seabed to the bedrock level at z_2. The soil–pile interaction is limited to a depth $z = L$ by a rigid boundary. The governing equations for the coupled system are discussed in greater detail in Tsouvalas and Metrikine (2014) and Peng et al. (2021) and are summarized in Eqs. (1), (2), and (3), which define the dynamic behavior of the pile, fluid, and soil domains under impact loading conditions:

$$\mathbf{L}\,\mathbf{u}_{pl} + \mathbf{I}_{\boldsymbol{m}}\ \ddot{\mathbf{u}}_{pl} = -\Big[H(z-z_1)\mathbf{t}_{\boldsymbol{s}} + \{H(z-z_0) - H(z-z_1)\}p_f + f_e\Big] \tag{1}$$

$$\nabla^2 p_f(r,z,t) - \frac{1}{c_f^2}\,\ddot{p}_f(r,z,t) = 0 \tag{2}$$

$$(\lambda + 2\mu)\nabla(\nabla\cdot\mathbf{u_s}) - \mu\nabla\times(\nabla\times\mathbf{u_s}) \tag{3}$$

The stiffness and inertia matrices are denoted by $\mathbf{L}$ and $\mathbf{I}_m$, respectively. The pile displacement is represented by the vector $\mathbf{u}_{pl}(z, t) = [u_{pl,r}, u_{pl,z}]^T$, where the subscript *pl* refers to the pile length, and *z* and *r* correspond to the vertical and radial directions. These displacement components describe the dynamic deformation of the pile in response to external loading. The circumferential (θ) displacement is omitted due to the assumption of axisymmetric. The external force acting on the ring surface of the pile is expressed as a vector $\mathbf{f}(z, t) = [f_{rr}, f_{rz}]^T$, comprising radial and shear traction components. The Heaviside function $H(z - z_i)$ is used to define the activation of the material interface at the depth separating the fluid and soil domains.

Equations (4) and (5) describe the velocity field in the acoustic fluid and the displacement field of the elastic soil medium, respectively.

$$\mathbf{v_f} = \nabla\phi_f \tag{4}$$

$$\mathbf{u}_s = \nabla\phi_s + \nabla\times\left(0, -\frac{\partial\psi_s}{\partial r}, 0\right) \tag{5}$$

By applying the Helmholtz decomposition together with the Fourier transform, these governing equations can be separated into components that distinctly characterize the propagation of compressional and shear elastic waves in the frequency domain as written in Eqs. (6) and (7).

$$\nabla^2\tilde{\phi}_f(r,z,\omega) = -\frac{\omega^2}{c_f^2}\tilde{\phi}_f(r,z,\omega) \tag{6}$$

$$\nabla^2\tilde{\phi}_s(r,z,\omega) = -\frac{\omega^2}{c_p^2}\tilde{\phi}_s(r,z,\omega) \quad \text{and} \quad \nabla^2\tilde{\psi}_s(r,z,\omega) = -\frac{\omega^2}{c_s^2}\tilde{\psi}_s(r,z,\omega) \tag{7}$$

Near-Field Modal Matching-Coupled Problem

The near-field modal matching technique is built upon the semi-analytical approaches developed by Peng et al. (2021) and Tsouvalas and Metrikine (2014). Each subsystem, namely the in vacuo shell and the fluid–soil domain, is represented in modal summation. The shell's in vacuo eigenmodes are obtained using the semi-analytical finite element formulation of Tsetas et al. (2023) within the following Love–Timoshenko thin-shell theory. As a result, the shell displacements encompassing both radial and axial motion are expressed as a modal summation in Eq. (8), where each mode individually satisfies the governing equations and boundary conditions of the shell structure.

$$\widetilde{u}_{pl,r}(z,\omega) = \sum_{m=1}^{\infty} A_{0m}\, U_{pl,r0m}(z) \;\text{ and }\; \widetilde{u}_{pl,z}(z,\omega) = \sum_{m=1}^{\infty} A_{0m}\, U_{pl,z0m}(z) \tag{8}$$

The modal constants A_{0m}, which remain unknown, are determined by solving the coupled system. The subscript m corresponds to the axial mode number. Specifically, the terms $U_{pl,r0m}$ and $U_{pl,z0m}$ represent the eigenvectors of the pile associated with radial and vertical motions, respectively.

The fluid and soil potential solution from Eqs. (6) and (7) that meets the boundary and interface conditions shown in Fig. 1 is expressed as a series expansion composed of modal summations. The fluid velocity and pressure are expressed as modal summations in Eqs. (9) and (10). Similarly, the soil displacement and stress are represented as modal summations in Eqs. (11), (12), and (13).

$$\widetilde{v}_{f,z}(r,z,\omega) = \sum_{p=1}^{\infty} C_p\, H_0^{(2)}(k_p r)\, v_{f,z,p}(z) \quad \text{and} \quad \widetilde{v}_{f,r}(r,z,\omega)$$

$$= \sum_{p=1}^{\infty} C_p\, H_1^{(2)}(k_p r)\, v_{f,r,p}(z) \tag{9}$$

$$\widetilde{p}_f(r,z,\omega) = \sum_{p=1}^{\infty} C_p\, H_0^{(2)}(k_p r)\, p_{f,p}(z) \tag{10}$$

$$\widetilde{u}_{s,z}(r,z,\omega) = \sum_{p=1}^{\infty} C_p\, H_0^{(2)}(k_p r)\, u_{s,z,p}(z) \text{ and } \widetilde{u}_{s,r}(r,z,\omega)$$

$$= \sum_{p=1}^{\infty} C_p\, H_1^{(2)}(k_p r)\, u_{s,r,p}(z) \tag{11}$$

$$\widetilde{\sigma}_{s,zz}(r,z,\omega) = \sum_{p=1}^{\infty} C_p\, H_0^{(2)}\left(k_p r\right)\, \sigma_{f,zz,p}(z) \;\text{ and }\; \widetilde{\sigma}_{s,zr}(r,z,\omega)$$

$$= \sum_{p=1}^{\infty} C_p\, H_1^{(2)}\left(k_p r\right)\, \sigma_{s,zr,p}(z) \tag{12}$$

$$\widetilde{\sigma}_{s,rr}(r,z,\omega) = \sum_{p=1}^{\infty} C_p\, \left(H_0^{(2)}\left(k_p r\right)\, \sigma_{s,rr,p}^{H_0}(z) + \frac{1}{r} H_1^{(2)}\left(k_p r\right)\, \sigma_{s,rr,p}^{H_1}(z)\right) \tag{13}$$

Similar to the modal decomposition used in the shell modal analysis, both the soil and fluid are characterized by unknown complex modal constants, denoted as C_p, which are subsequently determined by enforcing the interface conditions. The fluid velocity and pressure eigenvector are represented by $v_{f,z}$, $v_{f,r}$, and p_f, respectively. Soil displacement in the radial and vertical eigenvector is described by $u_{s,r}$ and $u_{s,z}$. The soil stress eigenvector, expressed as $\sigma_{s,zz}$, $\sigma_{s,zr}$, and $\sigma_{s,rr}$, is given in cylindrical coordinates. The functions $H_0^{(2)}$ and $H_1^{(2)}$ correspond to the Hankel functions of the first and second kinds, which model the propagation of cylindrical waves.

Pile–Soil and Pile–Fluid Interface Conditions Along the Radial Coordinate

The radial velocity of the fluid at the pile–fluid interface equals that of the shell structure as described in Fig. 1:

$$\begin{aligned} & i\,\omega\, \widetilde{u}_{pl,r}(z,\omega) = \widetilde{v}_{f,r}(R,z,\omega) \\ & i\omega \sum_{m=1}^{\infty} A_{0m}\, U_{pl,r,0m}(z) = \sum_{p=1}^{\infty} C_p\, H_1^{(2)}\left(k_p R\right)\, v_{f,r,p}(z) \end{aligned} \tag{14}$$

Likewise, the radial displacement of soil equals that of the shell structure at the interface:

$$\begin{aligned} & \widetilde{u}_{pl,r}(z,\omega) = \widetilde{u}_{s,r}(R,z,\omega) \\ & \sum_{m=1}^{\infty} A_{0m}\, U_{pl,r,0m}(z) = \sum_{p=1}^{\infty} C_p\, H_1^{(2)}\left(k_p r\right)\, u_{s,r,p}(z) \end{aligned} \tag{15}$$

Pile–Soil Interface Condition Along the Vertical Coordinate

A constitutive relation for the contact in the z-direction is introduced as shown in Fig. 1, illustrating the pile interacting with the soil–fluid system. At the pile–soil interface, a Kelvin–Voigt interface system is used, consisting of an elastic spring and

a dashpot, represented by k_{fi} and c_{fi}, respectively. The shear stress is expressed as a combination of the spring and dashpot responses, proportional to the relative displacement and velocity at the interface:

$$\begin{aligned}\widetilde{\sigma}_{s,zr}(z,R,\omega) &= -\left(k_{fi}+i\omega\, c_{fi}\right)\left(\widetilde{u}_{\mathrm{pl,z}}(z)-\widetilde{u}_{\mathrm{s,z}}(z,R)\right)\\ \widetilde{\sigma}_{s,zr}(z,R,\omega) &= -\left(k_{fi}+i\omega\, c_{fi}\right)\left(\sum_{m=1}^{\infty} A_{0m}\, U_{pl,z0m}(z)-\sum_{p=1}^{\infty} C_p\, H_0^{(2)}\left(k_p r\right)\, u_{s,z,p}(z)\right)\end{aligned} \tag{16}$$

Further elaboration of the expression above results in

$$\begin{aligned}\sum_{m=1}^{\infty} A_{0m}\, U_{pl,z0m}(z) = &-\frac{\sum_{p=1}^{\infty} C_p\, H_1^{(2)}\left(k_p r\right)\, \sigma_{s,zr,p}(z)}{\left(k_{fi}+i\omega\, c_{fi}\right)}\\ &+\sum_{p=1}^{\infty} C_p\, H_0^{(2)}\left(k_p r\right)\, u_{s,z,p}(z)\end{aligned} \tag{17}$$

In the case of the full pile–soil contact, the equation above simplifies to

$$\sum_{m=1}^{\infty} A_{0m}\, U_{pl,z0m}(z) = \sum_{p=1}^{\infty} C_p\, H_0^{(2)}\left(k_p r\right)\, u_{s,z,p}(z) \tag{18}$$

Full pile–soil contact, that is, $k_{fi} \to \propto$, yields the cancellation of the first term on the right-hand side of Eq. (17), effectively changing to the classical assumption of a perfect contact condition, where the vertical displacements of the soil and pile are equal. To determine the complex unknown model constants, the soil–fluid orthogonality condition is applied, as outlined in Tsouvalas and Metrikine (2014). The key modification in this formulation is the introduction of the interface spring and dashpot system, which captures the interaction between the pile and the surrounding elastic domain.

Case Study

This section studies how the contact mechanism between the pile and surrounding soil affects the particle motion. The study includes a sensitivity analysis emphasizing two extreme scenarios that are perfect contact and noncontact between the pile and the adjacent soil. Particular attention is given to cases involving large-diameter piles. The case study presented in Fig. 2 summarizes the main features and setup used for this analysis. The pile geometry, material properties, and loading conditions are summarized in Figure 2a and the loading function in Figure 2b.

A sensitivity analysis is conducted for three representative cases:

1. **Perfect contact** (Case PC), classical assumption where vertical displacement of pile and soil are identical
2. **Partial contact** (Cases A and B), finite stiffness interface (k_{fi}) and (c_{fi})
3. **Noncontact** (Case NC), vertical coupling between pile and soil is absent

Figures 3 and 4 illustrate the particle motion trajectories (hodographs) at the seabed interface and a height of 2 m above the seabed for both the soil and the surrounding fluid. It can be observed that in both the perfect contact and noncontact scenarios, the motion of water and soil exhibits an anticlockwise rotation. Under perfect contact conditions, the fluid trajectory forms a near-circular or cardioid shape, whereas the seabed motion is more constrained and elliptical. However, the form is more complex in the noncontact case deviating from typical elliptical paths unlike the perfect contact. The rip-slip behavior at the seabed is evident in both

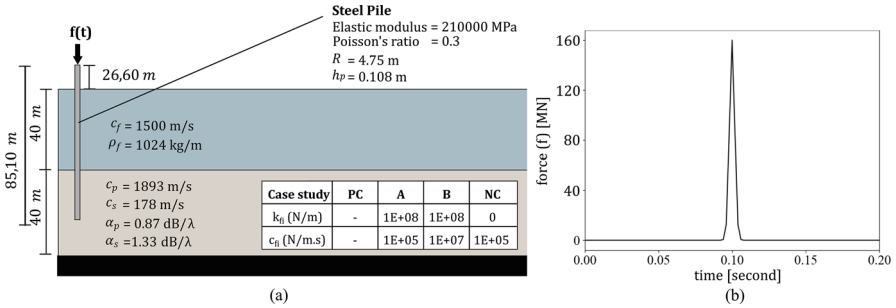

Fig. 2 The case study parameters: (**a**) the subsystems basic geometry, material properties, and the sensitivity analysis for pile–soil contact parameters; (**b**) the hammer force in time domain

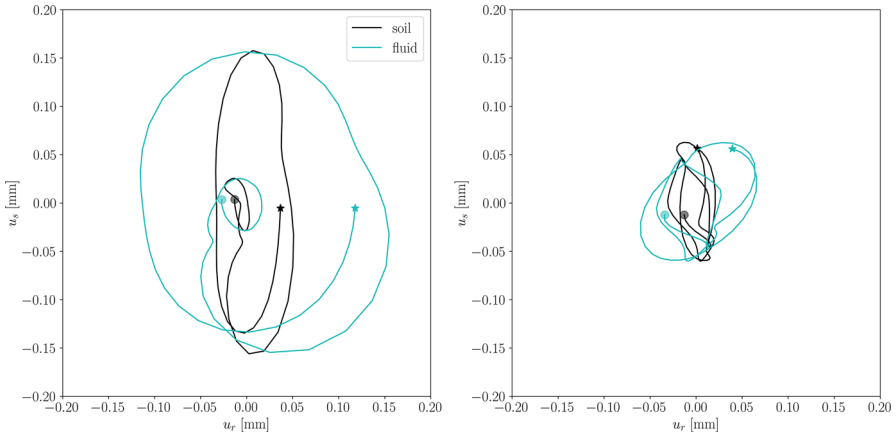

Fig. 3 Hodograph at fluid and soil particle motion trajectory at the seabed interface: (left) perfect contact condition; (right) noncontact condition. The circle mark denotes the starting point of motion, and the star mark denotes the ending point

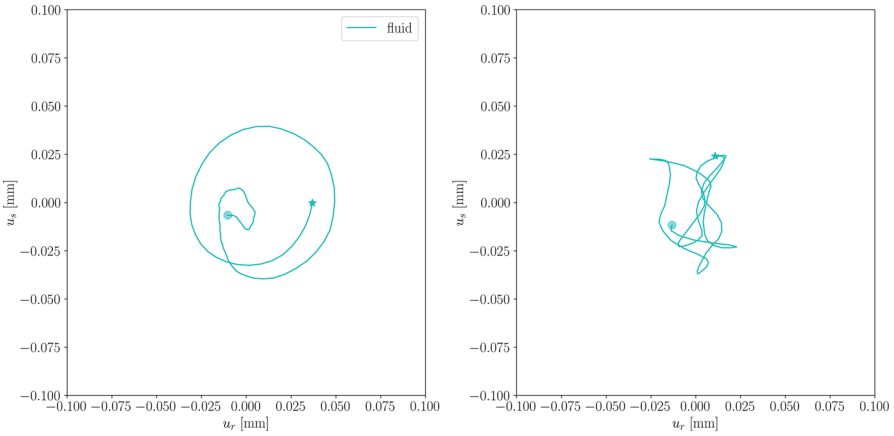

Fig. 4 Hodograph at fluid particle motion trajectory at the 2 m above seabed interface: (left) perfect contact condition; (right) noncontact condition. The circle mark denotes the starting point of motion, and the star mark denotes the ending point

hodographs, particularly in the plots of upward versus radial outward displacement as shown in Fig. 3. In terms of amplitude, the transient response generally under perfect contact conditions shows a greater magnitude compared to that of the noncontact condition.

Figure 5 presents the peak values of particle displacement (PPD), velocity (PPV), and acceleration (PPA) obtained from the sensitivity analysis conducted under varying pile–soil contact conditions in the near-field, radius of 40 m, and in the vicinity of seabed interface. The results indicate that as the mechanical coupling between the pile and the surrounding sediment is progressively reduced from perfect contact to partial or no contact, there is a corresponding decrease in the magnitude of particle motion parameters. Additionally, when the damping constant of c_{fi} is increased (as in Case B), the dynamic response of the pile is further suppressed. Under these conditions, the system's behavior begins to align with the result of the perfect contact scenario.

As depicted in Fig. 6, low-frequency oscillations are identified as Scholte interface waves. When linear slip is introduced at the pile–soil contact, the generation of Scholte waves is reduced, resulting in decreased particle motion amplitudes. This effect is also shown in Fig. 7 for acceleration distribution across the radius, demonstrating that pile–soil contact mechanics have a significant impact on particle motion in the near-field.

The effect of the interaction between the pile–soil presented in Fig. 7 is governed in the near-field region, where the pile–soil interaction strongly influences the acoustoelastic waves generated. For the representative monopile geometrical properties and soil conditions studied, the influence of pile contact linear slip is significant up to approximately 200 m and gradually diminishes beyond this distance, becoming negligible in the far field. At larger distances, environmental

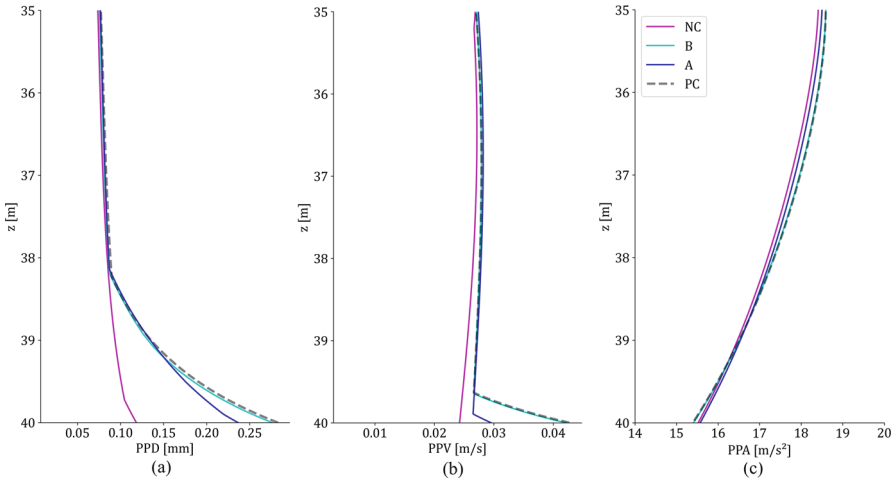

Fig. 5 Peak particle motion in radius 40 m and vicinity of the seabed with various contact mechanism between the pile and the surrounding soil: (**a**) peak particle displacement; (**b**) peak particle velocity; (**c**) peak particle acceleration

heterogeneity, such as soil stratigraphy and bathymetry variations, plays an increasingly dominant role and is studied in Peng et al. (2024) and Sertlek et al. (2024).

In the next section, potential effects on benthic species are examined by comparing observed values with sensitivity thresholds from the literature.

Particle Motion Possible Ecological Impact on Benthic Environments

Osteichthyes and cartilaginous fishes can detect low-frequency particle motion using the otolith organs in their ears (Popper and Hawkins 2019). Therefore, it is likely that fish living on or near the substrate can sense particle motion caused by substrate movement. For instance, Chapman and Sand (1974) recorded that the flatfish plaice (*Pleuronectes platessa*) is sensitive to water particle velocities as low as 0.3 μm/s at around 20 Hz. This value is notable when compared with the case study particle velocities, which reach up to 0.024–0.043 m/s at radius 40 m from the source as indicated in Fig. 5b.

Cones et al. (2022) demonstrated that pile-driving noise causes clear, but temporary, disruptions to squid swimming behavior with the experimental setup used smaller piles (0.3 m diameter). The pile diameter in the experiment is much smaller compared to the much larger piles (8–10 m diameter) used in offshore wind turbine monopile construction. Therefore, noise from actual projects is expected to be louder and affects a wider area, potentially causing more widespread and severe behavioral impacts. Additionally, experiments (Solé et al. 2017) demonstrate that cuttlefish exposed to sound levels between 139 and 142 dB re 1 μPa^2 at a 1/3 octave band

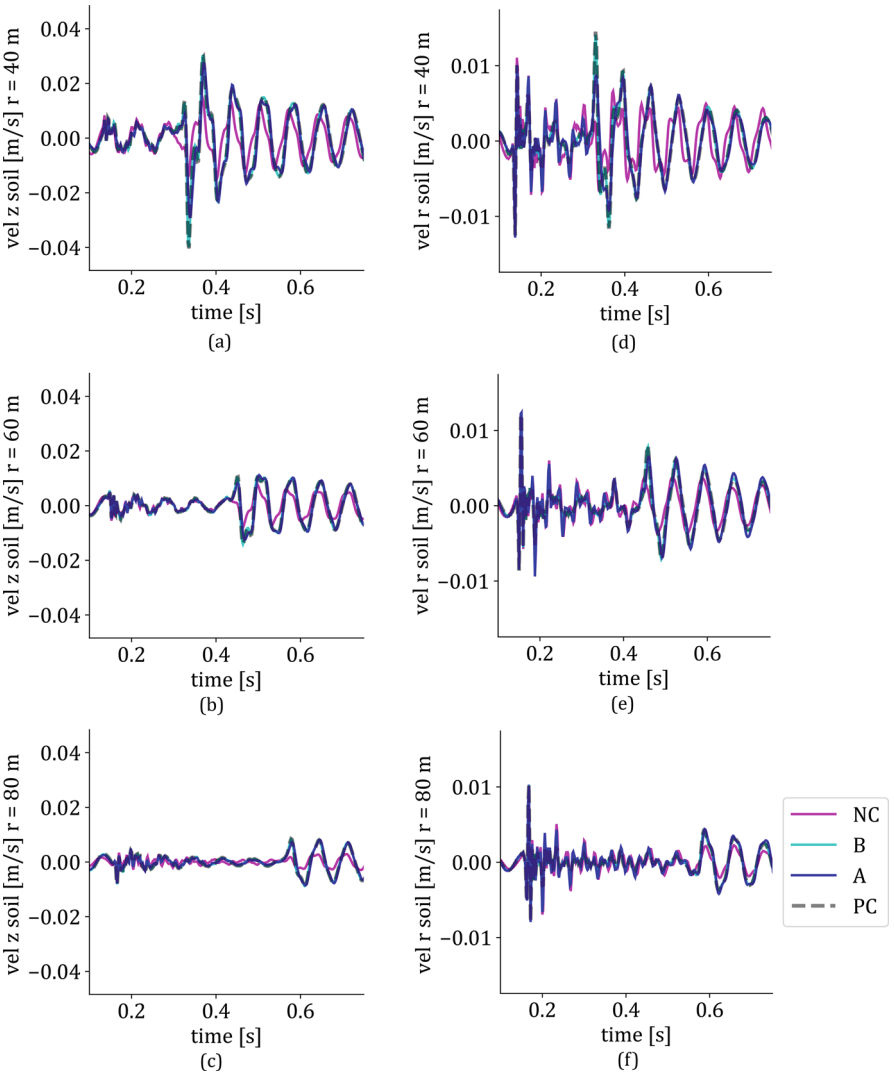

Fig. 6 The soil velocity in z-direction: (**a**) at radius 40 m, (**b**) radius 60 m and (**c**) radius 80 m; and the soil velocity in r-direction: (**d**) at radius 40 m, (**e**) radius 60 m and (**f**) radius 80 m

centered around 315 Hz, and between 139 and 141 dB re 1 μPa^2 at a 1/3 octave band centered around 400 Hz, along with particle motion acceleration peaks reaching 0.7 m/s^2, can experience traumatic injuries caused by the noise exposure. These values are particularly lower when compared to particle motion measurements in benthic environments, where accelerations as high as 3.35 m/s^2 have been extracted at a distance of 400 m from the source.

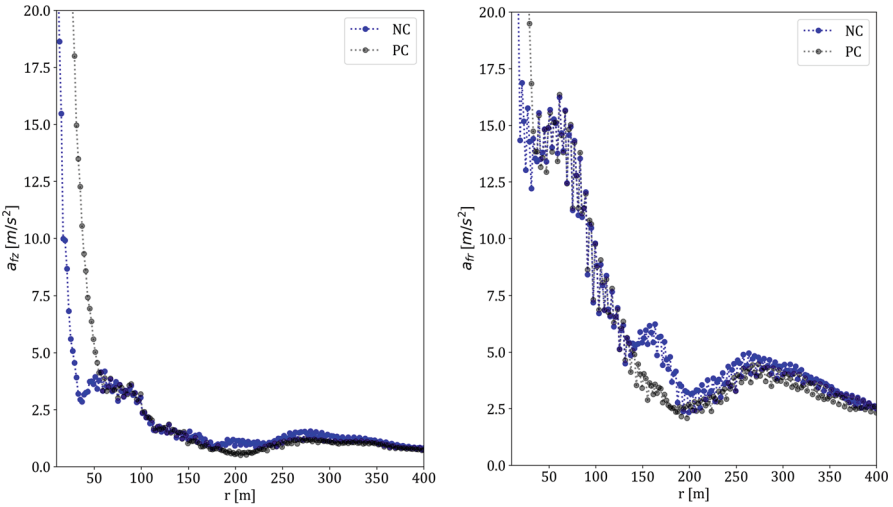

Fig. 7 Fluid peak acceleration: (**a**) vertical acceleration and (**b**) radial acceleration with radius distance from the source at the seabed level

Directional information from particle motion allows animals to pinpoint the position of sound sources, a key aspect of sound localization. This capability supports vital behaviors, including finding food, navigating through acoustic surroundings, maintaining spatial awareness, evading predators, and facilitating reproduction (Zeddies et al. 2012). Further research is needed to understand how certain types of directional motion might interfere with or disrupt these behaviors.

Conclusion and Future Works

Incorporating linear contact slip at the pile–soil interface significantly influences the characteristics of particle motion during pile-driving. It reduces both displacement and velocity in the adjacent soil and surrounding fluid, and introduces more complex, nonelliptical particle trajectories. Furthermore, acceleration near the source is generally lower. The effects of the contact mechanism diminish with increasing distance from the source.

Importantly, pile-driving in this case study, especially with larger-diameter piles and with its soil condition, can produce high levels of particle motion, acceleration, velocity, and displacement. The resulting velocities and accelerations exceed the sensitivity thresholds of benthic species as shown in the references. These exceeding values highlight the need for effective abatement systems that reduce sound pressure and address particle motion to help minimize potential impacts on marine life.

Future research will focus on calibrating the contact mechanism parameters through laboratory-scale and in situ experiments to improve predictive accuracy

under realistic conditions. Because pile–soil interaction during impact driving is inherently nonlinear, the use of a linear-equivalent approximation is applied to examine its effects on acoustoelastic waves in the coupled soil–water domain. Therefore, this linear interface system, which consists of a spring and a dashpot, must be calibrated against actual datasets. Additionally, the prediction model can be improved by incorporating depth- and frequency-dependent soil properties. This improvement aims to better capture the varied soil characteristics found in offshore environments. Further refinement of far-field predictions using the half-space domain eliminates artificial reflections introduced by rigid boundary assumptions. The model can be coupled with the far-field propagation such as to also include the spatial dependent heterogeneity (Peng et al. 2021, 2024; Sertlek et al. 2024). Finally, multidisciplinary efforts are needed to better understand the influence of particle motion on marine organism behavior and health. In addition to amplitude and frequency, engineering-relevant metrics such as exposure duration, distance from source, spatial dispersion patterns, and trajectory complexity should be quantified.

Acknowledgments The authors gratefully acknowledge SEASOUNDS for providing financial support for the research project. SEASOUNDS has received funding from the European Union's Horizon Programme under the Marie Skłodowska-Curie actions HORIZON-MSCA-2022-DN-01 (grant agreement ID: 101119769 research project).

Competing Interest Declaration The author(s) has no competing interests to declare that are relevant to the content of this manuscript.

References

Bohne T, Grießmann T, Rolfes R (2024) Comprehensive analysis of the seismic wave fields generated by offshore pile driving: a case study at the BARD offshore 1 offshore wind farm. J Acoust Soc Am 155(3):1856–1867. https://doi.org/10.1121/10.0025177

Chapman CJ, Sand O (1974) Field studies of hearing in two species of flatfish *Pleuronectes platessa* (L.) and *Limanda limanda* (L.) (family Pleuronectidae). Comp Biochem Physiol A Physiol 47(1):371–385. https://doi.org/10.1016/0300-9629(74)90082-6

Cones SF, Jézéquel Y, Ferguson S, Aoki N, Mooney TA (2022) Pile driving noise induces transient gait disruptions in the longfin squid (*Doryteuthis pealeii*). Front Mar Sci 9:1070290. https://doi.org/10.3389/fmars.2022.1070290

Molenkamp T, Tsetas A, Tsouvalas A, Metrikine A (2024) Underwater noise from vibratory pile driving with non-linear frictional pile-soil interaction. J Sound Vib 576:118298. https://doi.org/10.1016/j.jsv.2024.118298

Peng Y, Tsouvalas A, Stampoultzoglou T, Metrikine A (2021) A fast computational model for near- and far-field noise prediction due to offshore pile driving. J Acoust Soc Am 149(3):1772–1790. https://doi.org/10.1121/10.0003752

Peng Y, Tsetas A, Molenkamp T, Sertlek O, Tsouvalas A (2024) Underwater sound modelling and sound mapping in vibratory pile driving. In W. van Keulen, & J. Kok (Eds.), Proceedings of the 30th International Congress on sound and vibration article 715 (Proceedings of the International Congress on Sound and Vibration). Society of Acoustics

Popper AN, Hawkins AD (2019) An overview of fish bioacoustics and the impacts of anthropogenic sounds on fishes. J Fish Biol 94(5):692–713. https://doi.org/10.1111/jfb.13948

Sertlek O, Peng Y, Tsouvalas A (2024) Modelling pile-driving sound and mitigation in realistic environments. In: Popper AN, Sisneros J, Hawkins AD, Thomsen F (eds) The effects of noise on aquatic life. Springer International Publishing. https://doi.org/10.1007/978-3-031-10417-6_149-1

Solé M, Sigray P, Lenoir M, Van Der Schaar M, Lalander E, André M (2017) Offshore exposure experiments on cuttlefish indicate received sound pressure and particle motion levels associated with acoustic trauma. Sci Rep 7(1):45899. https://doi.org/10.1038/srep45899

Solé M, Kaifu K, Mooney TA et al (2023) Marine invertebrates and noise. Front Mar Sci 10: 1129057. https://doi.org/10.3389/fmars.2023.1129057

Tsetas A, Tsouvalas A, Metrikine AV (2023) A non-linear three-dimensional pile-soil model for vibratory pile installation in layered media. Int J Solids Struct 269:112202. https://doi.org/10.1016/j.ijsolstr.2023.112202

Tsouvalas A, Metrikine AV (2014) A three-dimensional vibroacoustic model for the prediction of underwater noise from offshore pile driving. J Sound Vib 333(8):2283–2311. https://doi.org/10.1016/j.jsv.2013.11.045

Zeddies DG, Fay RR, Gray MD, Alderks PW, Acob A, Sisneros JA (2012) Local acoustic particle motion guides sound-source localization behavior in the plainfin midshipman fish, *Porichthys Notatus*. J Exp Biol 215(1):152–160. https://doi.org/10.1242/jeb.064998